Textures of Continuously Annealed IF Steels

Professor Dr. Dierk Raabe

Max-Planck-Institut für Eisenforschung
Max-Planck-Str. 1
40237 Düsseldorf
Germany
(raabe@mpie.de)

Summary

The crystallographic textures and the resulting plastic anisotropy of five IF (interstitial free) steels with different carbon equivalents and Nb and Ti microalloying content have been investigated. The steels were industrially hot rolled, cold rolled, annealed, and finally hot–dip galvanized. An alternative heat treatment of the cold rolled samples was conducted in laboratory scale using parameters close to those in industry–scale continuous annealing lines. The anisotropy parameters were both measured and predicted on the basis of the measured texture data. The calculated $\bar{r}$–values were corrected by using functions which were fitted to the experimental data. It was found that for a given hot and cold rolling state even minor changes in the annealing conditions can improve the anisotropy parameter $\bar{r}$ by up to 13 %. Increase in recrystallization texture and improvement of the resulting anisotropy parameters are discussed in terms of partial transformation of ferrite to austenite in the intercritical regime.

I. Introduction

High values of the average plastic sheet anisotropy, commonly described by the engineering parameter $\bar{r}$, and minimum in–plane orientation dependence of the anisotropy parameter, usually referred to as Δr, are among the predominant objectives in optimizing the properties of IF (interstitial free) steel sheets. Beneficial combinations of both parameters typically entail a high in–sheet plastic isotropy and a good deep drawability.

The plastic anisotropy parameter for a given stress–strain state is described by the ratio of broadening to thickness reduction of a flat sample. The kinematic portion of the plastic anisotropy can be calculated from the crystallographic texture of the sheet. Calculation methods for plastic anisotropy parameters are commonly based on appropriate homogenization theory such as Taylor–Bishop–Hill [1–3] and self–consistent approaches or discrete single–component based methods such as crystal plasticity finite element methods [4].

Crystallographically, plastic anisotropy originates from the discreteness of crystal slip in each of the grains constituting a polycrystalline material. The directionality of crystal slip with respect to the external reference frame, imposed by the actual deformation state, is determined by the texture. The texture provides a quantitative relation between the crystal reference systems of all the individual grains and the external reference system exerted by the process. This implies that conventional deep drawing property quantities are only valid for one particular velocity gradient tensor. This aspect is of particular relevance when Taylor–Bishop–Hill–type or self–consistent–based strain rate homogenization models serve for predicting deep drawing properties. In other words it is conceivable that a given texture may provide beneficial deep drawing properties for one particular deformation state while it might have worse properties for another. Deep drawability for intricate deformation paths is thus better computed by use of discrete crystal plasticity theory. Optimum deep drawing behavior of IF steels under ideal, homogeneous plane-strain conditions is obtained by a strong and homogeneous {111}<uvw> fiber texture (γ–fiber) [5–8].

Textures of steel sheet products are affected by all production steps, i.e. by hot rolling, cold rolling, and final continuous annealing. Cold rolling textures of body centered cubic (bcc) transition metals have been widely investigated by experiment [5–10] and simulation [6–17]. In recent years, recrystallization textures of IF steels have been studied extensively and also modeled [18–29]. Steels, which are to be zinc coated, are usually annealed in a continuous line, that includes recrystallization and subsequent hot–dip galvanizing in one consolidated process. In these kinds of processes, the annealing parameters can be controlled by adjusting the line speed and temperatures in the processing zones.

The aim of this report is to investigate and optimize the normal anisotropy of IF steel sheets by means of enhancing the overall level and homogeneity of the {111}<uvw> texture. We investigate the texture and anisotropy of five IF steels with different carbon equivalents and different Nb and Ti microalloying contents. All parameter variations in this work are conducted within a range feasible at the industrial scale.

II. Experimental

A. *Sample processing*

Five IF steels were investigated. Their chemical compositions are given in Table 1. Steels 1–3 are Ti–stabilized, steel 4 is Ti and Nb stabilized, and steel 5 is a Ti and Nb stabilized high–strength IF steel.

Table 1. Chemical compositions of the investigated steels (mass contents in %)

Steel	C	N	Si	Mn	P	S	Al	Nb	Ti	B
1	0.0030	0.0077	0.005	0.093	0.004	0.0037	0.036	0.013	0.081	0.0001
2	0.0036	0.0029	0.012	0.106	0.006	0.0042	0.055	0.002	0.094	0.0002
3	0.0027	0.0038	0.006	0.084	0.005	0.0039	0.039	0.002	0.114	0.0001
4	0.0040	0.0034	0.009	0.146	0.006	0.0067	0.043	0.041	0.028	0.0000
5	0.0034	0.0040	0.005	0.405	0.051	0.0040	0.041	0.033	0.026	0.0008

All steels were industrially exposed to slab reheating at 1523 K. Subsequent hot rolling was conducted above the A_{r3}–temperature with final coiling temperatures of 973 – 993 K (Table 2). The hot band thickness prior to cold rolling was between 2.5 – 3 mm. Cold rolling was performed in an industrial tandem line with four roll stands. The accumulated technical thickness reduction during cold rolling varied between 59 % and 78 %. After cold rolling steels all were industrially annealed at 1113 K in a continuous line and finally hot–dip galvanized. Relevant industrial process parameters are given in Table 2.

Table 2. Industrial process parameters

Steel	1	2	3	4	5
Slab reheating T [K]	1523	1523	1523	1523	1523
Hot rolling finishing T [K]	1178	1198	1198	1188	1183
Coiling T [K]	973	973	973	993	993
Hot band thickness, mm	3.0	3.0	3.0	2.5	3.0
Cold rolling reduction, Δd/d %	75	78	75	74	59
Cold band thickness, mm	0.80	0.70	0.80	0.70	1.25
Annealing T [K]	1113	1113	1113	1113	1113
Zinc coating, g/m2	275	275	275	275	275

The effect of heat treatment on sheet recrystallization was further investigated for cold rolled steels 1 and 3 at laboratory scale using process variations which are feasible also at the industrial scale. For this purpose 120 × 25 mm^2 samples were cut out of cold rolled sheets and annealed using the Gleeble 1500 thermomechanical simulator. Six different thermal cycles which can be realized in continuous annealing lines were used, Figure 1. Maximum temperatures of cycles varied between 1053 K to 1133 K and the total annealing times varied between 90 to 210 seconds.

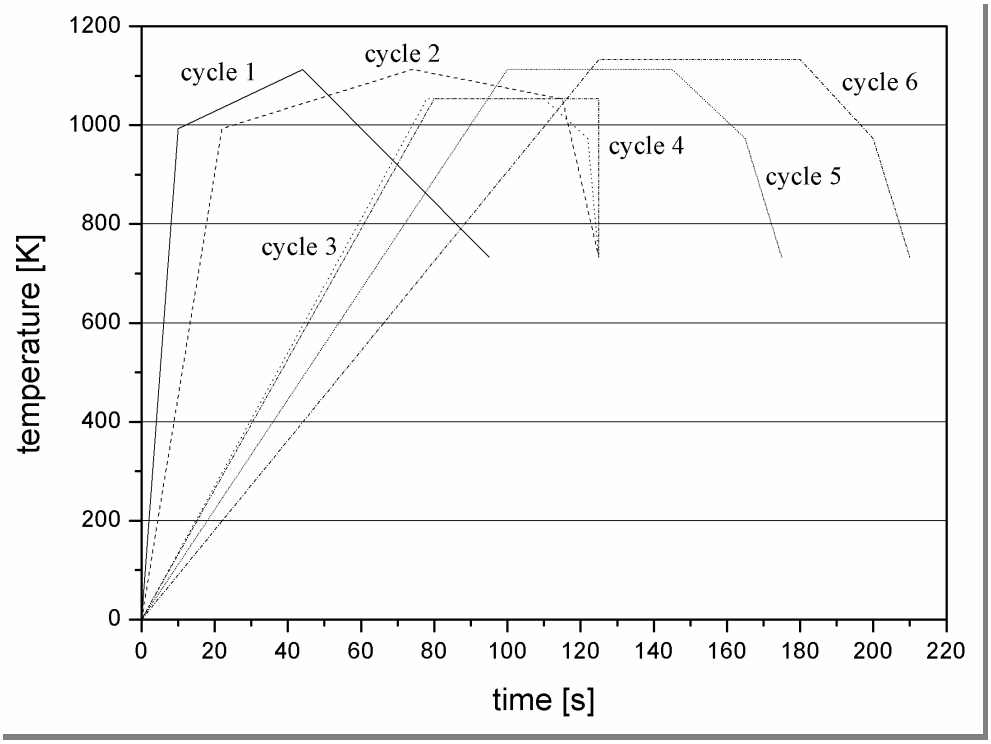

Figure 1. Six different annealing treatments applied to the cold rolled steels. All annealing schemes can be realized at industry scale.

B. Texture and anisotropy analysis

Since textures of steels often vary through the sample thickness, crystallographic textures of hot bands, cold rolled bands and final annealed sheets were investigated in two different through–thickness layers, described by s = 0 and s = 0.8. The parameter s is defined by the spacing between the inspected layer and the sheet center layer, counting positive from the center layer, divided by the half thickness, i.e. s = 0 indicates the center layer while s = 0.8 indicates the sub–surface layer.

Samples for pole figure measurement were mechanically prepared by grinding the material to within 10 μm–15 μm of the investigated layers. The final material was etched by HF prior to the measurement. All pole figures were determined by measuring the four incomplete pole figures {110}, {200}, {112} and {103} in the back reflection mode using $Mo_{K\alpha 1}$ radiation [30]. In the pole figures RD is the rolling direction, ND the normal direction, and TD the transverse direction of the original sheet sample. From these pole figure data the orientation distribution functions (ODFs) were calculated using a series expansion method. The employed ODF technique was based on spherical harmonics using an expansion degree of l_{max}=22 [31]. This expansion degree is appropiate for pole figure source data with a grid resolution of 5°×5°. In the ODF the texture is at each point represented in the form of an orientation density f(g) in Euler space where the orientation g is here given in terms of the Euler angles φ_1, ϕ, and φ_2.

According to the cubic crystal symmetry and the approximate orthorhombic sample symmetry the textures are presented in the reduced Euler space ($0° \leq \varphi_1, \phi, \varphi_2 \leq 90°$). The application of the ODF for texture and anisotopy analysis is superior to the use of pole figures. The latter represent 2-dimensional projections along some crystallographic path through the 3-dimensional orientation space. This means that pole figures have a higher degree of ambiguity when compared to the ODF.

BCC metals tend to develop pronounced orientation densities around or close to certain symmetric crystallographic axes. These orientation tubes in orientation space are referred to as texture fibers. The most important texture fibers are given in Table 3 [32,33].

Table 3: Relevant fibers for the description of textures of BCC transition metals [32,33]

Fiber	Fiber axis	Relevant texture components on the fiber
α–fiber	<110> ¦ RD	{001}<110>–{112}<110>–{111}<110> (incomplete fiber)
γ–fiber	<111> ¦ ND	{111}<110>–{111}<112>
η-fiber	<001> ¦ RD	{001}<100>–{011}<100>
ζ–fiber	<011> ¦ ND	{011}<100>–{011}<211>–{011}<111>–{011}<011>
ε–fiber	<110> ¦ TD	{001}<110>–{112}<111>–{111}<112>–{011}<100>
θ–fiber	<001> ¦ ND	{001}<100>–{001}<110>

RD: rolling direction, ND: normal direction, TD: transverse direction

Anisotropy values (Lankfort values, r–values) of the hot bands and industrially cold rolled and annealed samples were measured in 0°, 45° and 90° angles to the rolling direction. From these the average anisotropy parameters $\bar{r}$ were calculated. Theoretical $\bar{r}$-values of industrial samples were calculated on the basis of texture data assuming pencil glide and compared to experimental ones. In these calculations the texture of the sub–surface layer was weighted with 40% and that of the

center layer with 60% in accordance with earlier work on hot band textures [33,34]. Anisotropy parameters of the laboratory annealed samples were also calculated and then corrected by the correlation obtained from the data of industrial samples.

III. Results

The hot band textures of all investigated steels were weak and in part close to random. Figure 2 exemplary shows the hot band texture of steel 3 in two through–thickness layers. While the sub–surface layer reveals a nearly random texture the center layer shows a weak {001}<110> components spread out towards {112}<110>. Furthermore, a weak isolated {554}<225> orientation appears on the ε–fiber.

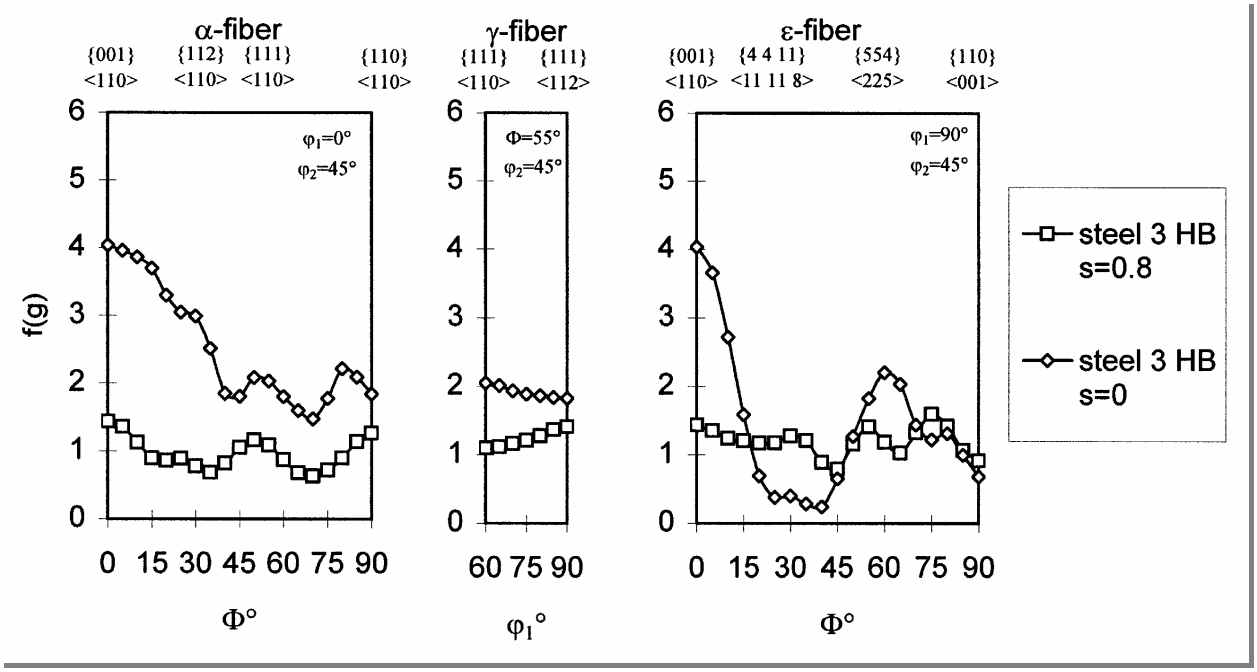

Figure 2. Hot band texture of steel 3 in two through–thickness layers (s = 0: center layer, s = 0.8: sub–surface layer).

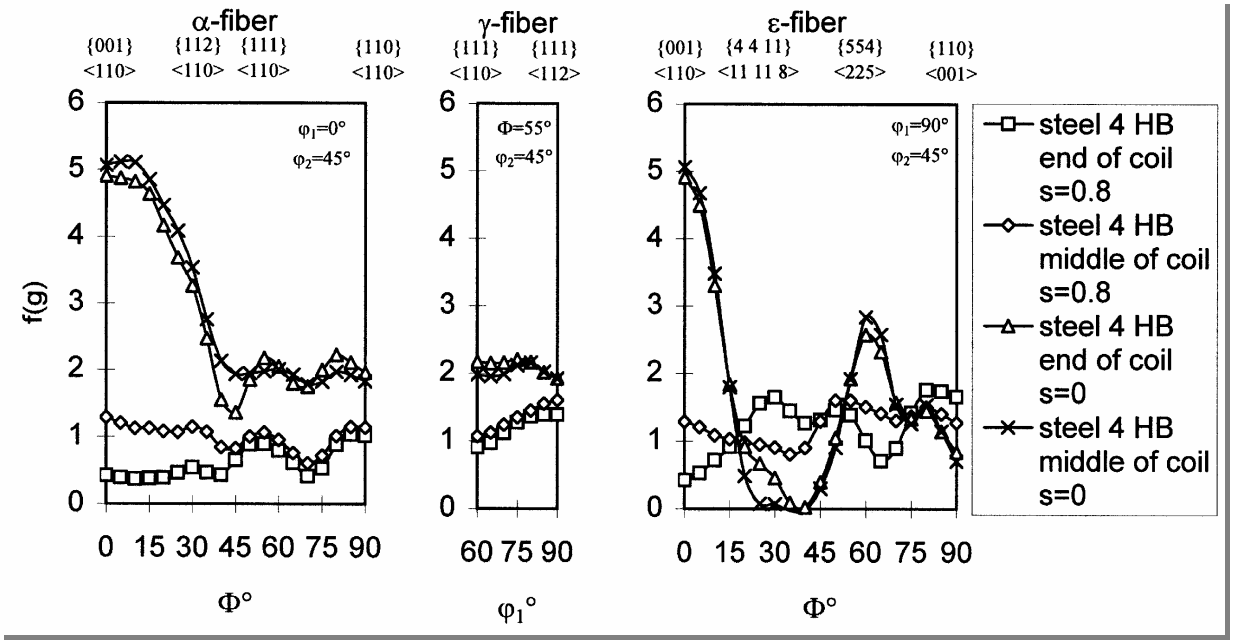

Figure 3. Comparison of hot band textures from samples taken at different in–plane positions (end of coil, middle of coil) of as hot rolled steel 4 (s = 0: center layer, s = 0.8: sub–surface layer).

Figure 3 shows a comparison of the hot band textures from samples taken at different in–plane positions (end of coil, middle of coil) of the hot rolled sheet of steel 4. The data show first that the textures are very similar to those observed in steel 3 (figure 2) and secondly that the inspected coil does not reveal any significant in–plane texture variation.

After cold rolling, the textures in all investigated steels are seen to be dominated by a strong α–fiber and a weaker γ–fiber. The maximum of the α–fiber is always close to the {112}<110> orientation. Due to the high cold rolling reductions, the textures reveal only minor discrepancies between the different thickness layers. In all cases the texture is stronger in the center than in the sub–surface layer. This applies particularly to the {001}<110> and {112}<110> components on the α–fiber, and, to a much smaller extent, to the γ–fiber. Figure 4 exemplary shows the texture of 75% cold rolled steel 3 in two through–thickness layers.

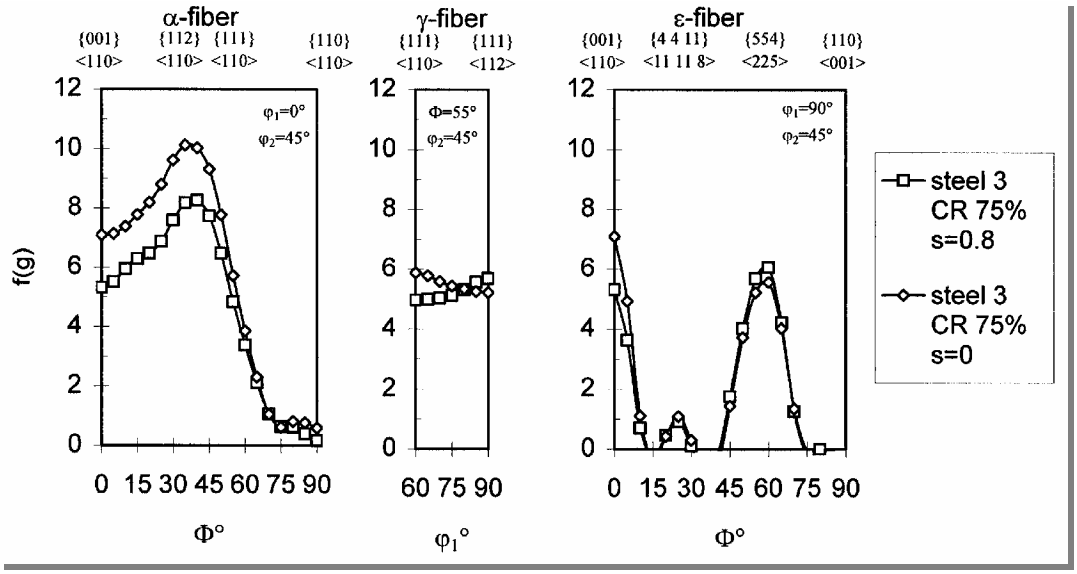

Figure 4. Texture of 75% cold rolled steel 3 in two through–thickness layers (s = 0: center layer, s = 0.8: sub–surface layer).

Annealing the industrially cold rolled sheets leads to significant changes in the texture of all investigated steels. Except for a strong component close to {111}<110> the orientation density of the α–fiber drops and the γ–fiber becomes dominant. On the γ–fiber the {111}<112> component is usually stronger than the {111}<110> component. The annealing textures at center layer and at sub–surface layer of each specimen were very similar. As the preceding degree of cold rolling increases, the γ–fiber texture after annealing becomes stronger (Figures 5,6).

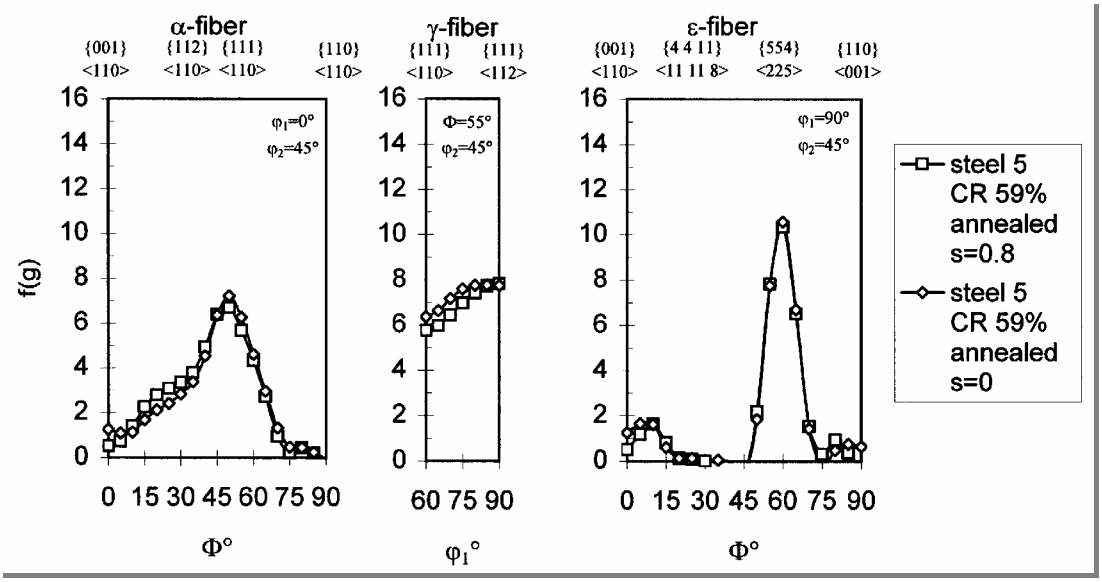

Figure 5. Texture of 59% cold rolled and annealed (1113 K) steel 5 in two through–thickness layers (s = 0: center layer, s = 0.8: sub–surface layer).

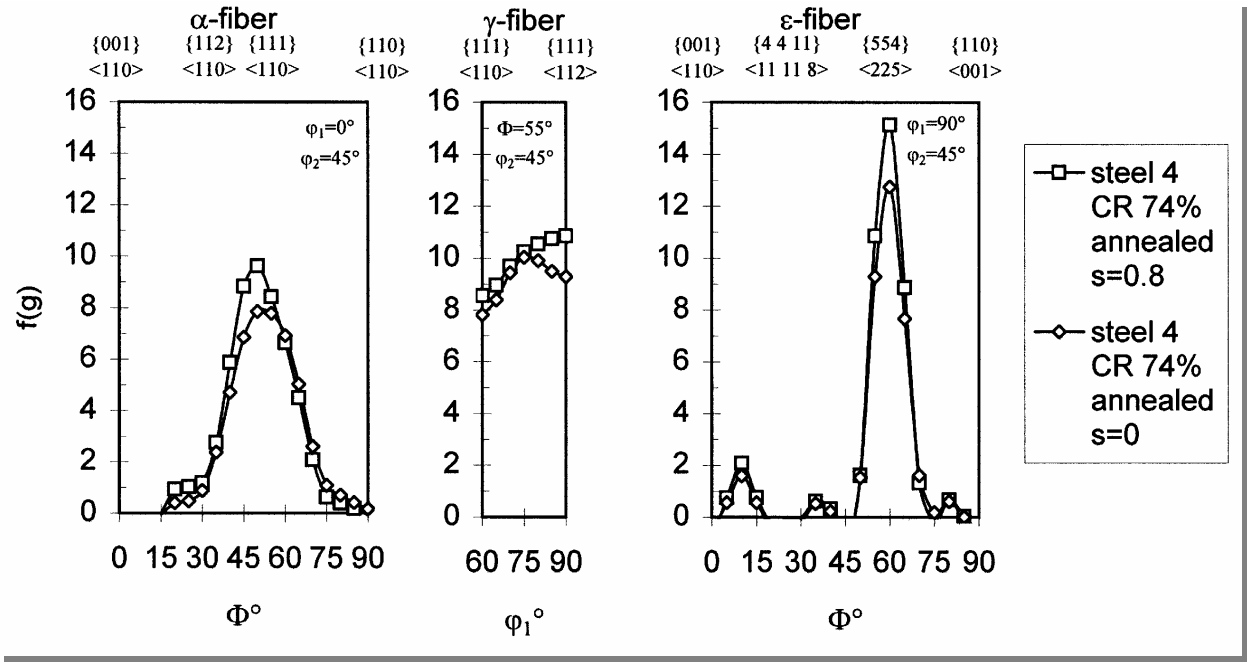

Figure 6. Texture of 74% cold rolled and annealed (1113 K) steel 4 in two through–thickness layers (s = 0: center layer, s = 0.8: sub–surface layer).

The textures of the laboratory heat treated samples of steels 1 and 3 (Figures 7–10) are similar to the textures of industrially produced sheets. Again, the γ–fiber texture after annealing dominates the overall texture. Comparing Figure 7 to Figure 8 reveals that steel 1 does not show any significant differences between the two different through–thickness layers.

Also, the textures arising from the various annealing cycles (cycles 1–6 are given in Figure 1) lead to practically identical textures, except for some minor variations which, however, are within the scatter width of the in–plane texture variation and the pole figure experiments. This is different for steel 3, where annealing cycle 6 produces a markedly sharper γ–fiber in comparison to the other five heat treatments which have nearly identical textures (Figures 9,10). Furthermore, steel 3 reveals a slightly sharper γ–fiber texture in the sub–surface layer than in the center layer.

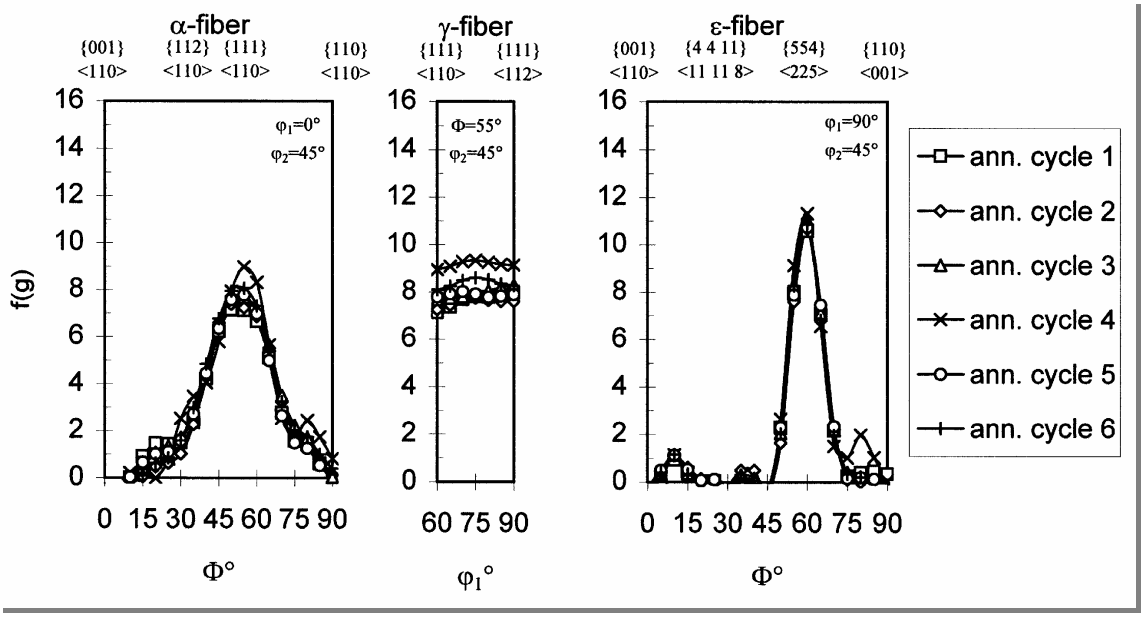

Figure 7. Texture of 75% cold rolled and annealed steel 1 in sheet center layer (s = 0). The different annealing schemes are given in figure 1.

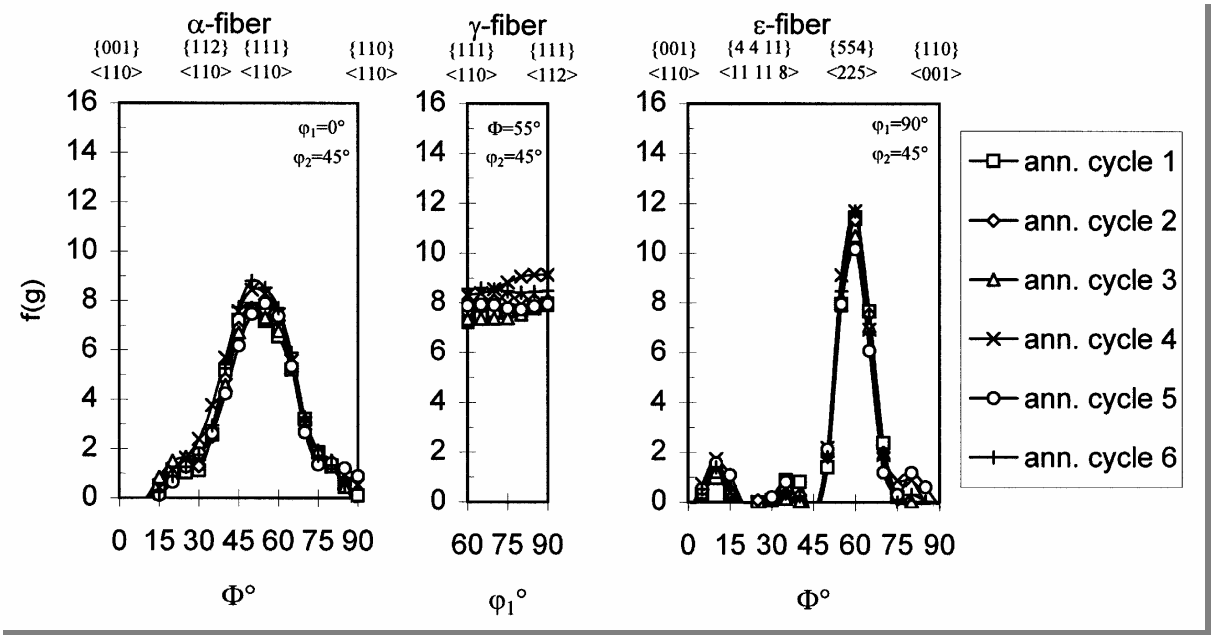

Figure 8. Texture of 75% cold rolled and annealed steel 1 in sheet sub–surface layer (s = 0.8). The different annealing schemes are given in figure 1.

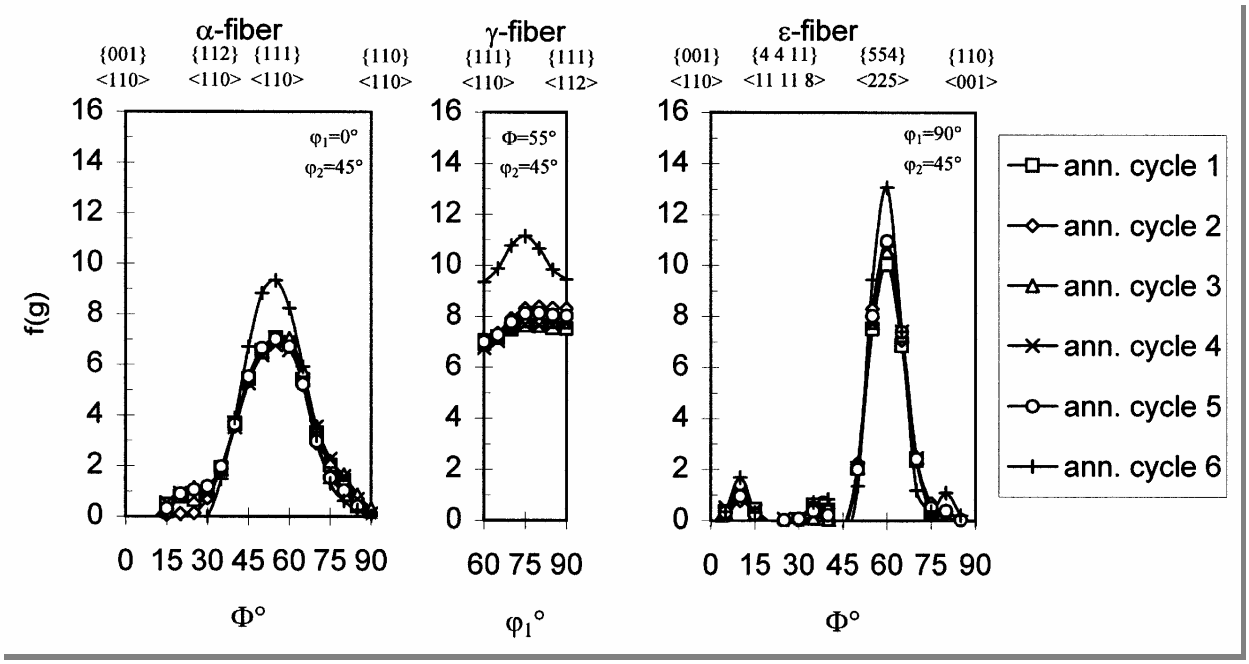

Figure 9. Texture of 75% cold rolled and annealed steel 3 in sheet center layer (s = 0). The different annealing schemes are given in figure 1.

IV. Discussion

A. Hot rolling texture

It is known from previous work on IF steels that the orientation distribution observed in hot rolled sheet shows nearly random sub–surface texture and a very weak α–fiber texture in the center layer. This is presumably due to phase transformation and partial recrystallization. Increases in hot band texture sharpness occur with increasing number of deformation steps conducted in the ferritic regime during hot rolling [34–41], Table 4.

Table 4. Main parameters which lead to different classes of hot band steel textures

Main groups of influence parameters on hot band steel textures	Main factors in each parameter group
group 1 (processing)	• casting conditions (e.g. continuous casting, thin strip casting) • slab treatment (e.g. slab annealing temperature, soaking time) • pre-rolling • hot rolling schedule (e.g. ferritic rolling, austenitic rolling, reduction scheme, macroscopic through-thickness strain rate profiles)
group 2 (thermodynamics)	• amount and kind of alloying elements • impurities • stored deformation energy • transformation behavior • stacking fault energy (austenite)
group 3 (microstructure)	• grain size and shape • recrystallization temperature and time • shear banding • precipitations
group 4 (crystallography)	• active slip systems • inherited textures • orientation relationships during transformation (e.g. Bain or Nishi-yama-Wassermann)

Commercial hot rolling conditions always lead to a strong through–thickness gradient in the displacement field creating a pronounced profile of shear and strain energy. While deformation in the center layer is close to a plane strain state, layers closer to the surface undergo strong shear deformation and accumulate more deformation energy. Also, the band during hot rolling is always colder close to the surface than in the center layer. In cases where most hot rolling steps are in the austenitic regime, these strain and temperature gradients lead to earlier transformation and stronger recrystallization in the sub–surface layer, entailing nearly complete texture randomization, and a somewhat more pronounced, in part recovered, weak α–fiber texture in the center layer (Figure 2). The investigated textures are thus typical examples of non–ferritic hot rolled low carbon and IF steels. Ferritic hot rolling of such products usually leads to more pronounced hot band textures, particularly in the sheet center layers [34–41].

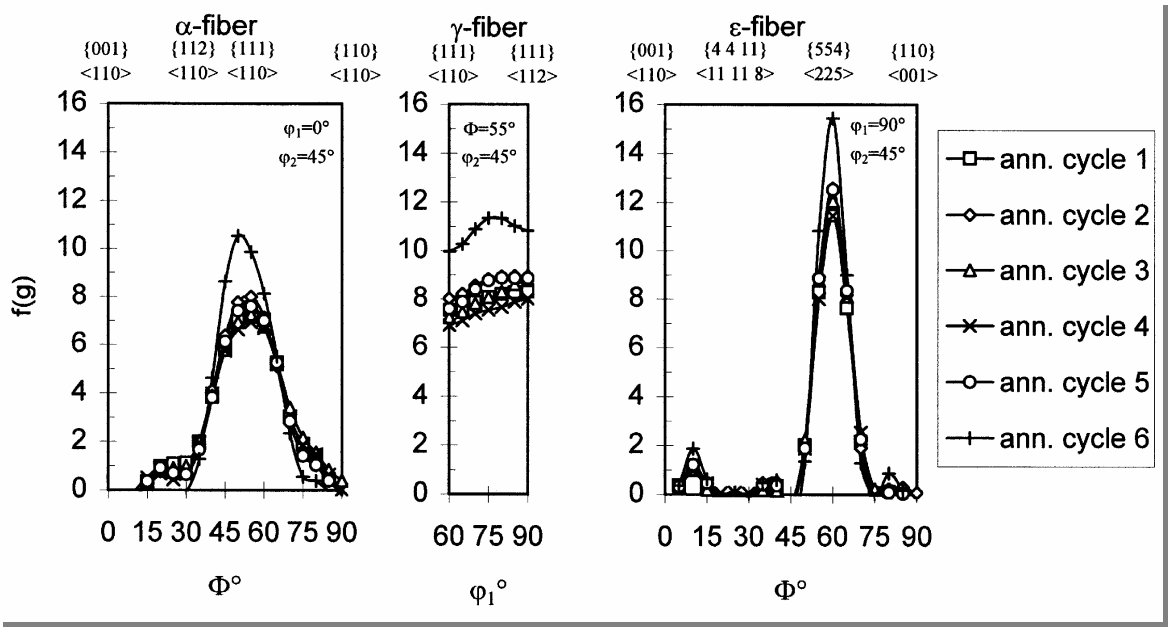

Figure 10. Texture of 75% cold rolled and annealed steel 3 in sheet sub–surface layer (s = 0.8). The different annealing schemes are given in figure 1.

The higher the hot rolling temperature is, the higher is usually also the in–plane hot band texture homogeneity. Ferritic hot rolling, as encountered in certain low carbon and IF steel processing lines or in highly Cr–alloyed ferritic stainless steels, usually produces stronger texture variation in the same coil. In samples inspected in this study, the hot band textures were very homogeneous throughout the coil (Figure 3).

It was shown in previous works that the crystallographic texture is usually a more sensitive indicator for hot band homogeneity than the grain microstructure [34–41]. Hot band texture serves as a starting texture for cold rolling and subsequent recrystallization. In–plane hot band homogeneity is thus an essential precondition for constant rolling and annealing textures, and hence, for constant deep drawing properties over the entire coil. Earlier investigations on different steels revealed that hot band material often shows strong texture variations within the same coil.

B. Cold rolling texture

The observed cold rolling textures with a strong α–fiber and a weaker γ–fiber (Figure 4) can be explained in terms of the slip systems activated in the different grains during the imposed near plane-strain deformation state and the grain reorientations resulting from it. Taylor–Bishop–Hill–based strain rate homogenization simulations based on the activation of {110}, {112}, and {123} slip planes with a common Burgers vector parallel to <111> very closely resemble the texture evolution found in most low carbon steels, provided the starting textures are properly taken into account as initial orientation distribution [14,16,42]. Accordingly, the observed somewhat sharper α–fiber texture in the center layer (Figure 4) can be associated with the initially slightly sharper texture in the hot band (Figure 2).

C. Recrystallization texture

According to Figure 1, all heat treatments of the cold rolled samples produced essentially recrystallized microstructures with typical recrystallization textures. Differences in the recrystallization textures are due to variation in the inherited hot band texture, the cold rolling texture, and the details of the annealing cycles.

Although the textures in both layers inspected are in most cases quite similar after cold rolling and annealing, the deformation history of the dominant cold rolling texture components should be considered for the discussion of the recrystallization behavior. The initial {001}<110> texture component formed during the last hot rolling steps is a recovered orientation with little deformation energy, close to zero reorientation rate during further cold rolling, very low Taylor factor, and with very symmetric, homogeneous and little kinematic slip activity during plane-strain rolling. Grains belonging to this inherited hot band component (center layer) are thus very slow to accumulate deformation energy during cold rolling and are therefore extremely reluctant to recrystallize during continuous annealing. {001}<110> oriented grains, however, which are not inherited from hot rolling (sub–surface layer), but form during cold rolling by gradual reorientation through orientation space following the plane-strain flow field, usually accumulate much higher strain energy and are therefore more prone to recrystallize. This difference makes clear that typical texture behavior is not simply a static characteristic which pertains to a certain orientation, but a history–dependent quantity depending on both orientation and strain path. This circumstance might ex-

plain why recrystallization textures are sometimes found to be sharper in the sub–surface layer than in the center layer (e.g. Figures 6, 9, 10) [43,44].

In most cases variations in the annealing treatment do not affect the recrystallization texture markedly (Figures 7, 8). This is not true for steel 3, where annealing cycle 6 entails a significantly sharper γ–fiber when compared to the other five cycles (Figures 9, 10). The results for steel 3 were confirmed on a separate sample. A possible explanation for this improvement lies in partial austenitization, rendering the annealing process intercritical. Compared to steel 1, steel 3 has a slightly lower carbon content. According to the Fe–C phase diagram at 1133 K, both steels are still in the α region. However, considering the other alloying elements in form of carbon equivalent (Table 1) shifts equilibrium towards the two–phase regime for cycle 6 with the highest annealing temperature. Several formulas exist for the calculation of the carbon equivalent [45]. For steels 1 and 3 they give results of 0.010 – 0.034 equivalent mass % and 0.010 – 0.054 equivalent mass %, respectively. Using these estimates suggests that at 1133 K steel 1 could contain 0 – 5 vol. % austenite and steel 3 even 0 – 15 vol. %. Partial transformation during annealing, which is referred to as intercritical annealing, has indeed been reported to increase sharpness of the γ–fiber texture [29]. Because of this point an attempt was made to detect partial transformation in steels 1 and 3 also by aid of metallography. However, after annealing at 1133 K and subsequent quenching no martensite was observed by optical microscopy.

D. Plastic anisotropy

The experimentally observed $\bar{r}$–values increase with increasing γ–fiber orientation density and preceding cold rolling reduction. Correlation of crystallographic texture and plastic anisotropy for industrial application requires quantitative procedures. Since theoretical models of the Lankfort value often show deviation from the experimentally observed ones, empirical fitting methods still prevail. A classical procedure consists in relating the intensity ratio of (111) and (001) planes from the texture measurement to the experimentally observed average strain ratio $\bar{r}$ and extracting an empirical function from that. This results from applying this procedure are shown in Figure 11, where all industrial hot bands and annealed cold bands whose anisotropy was measured are taken into account. The mean value of γ–fiber orientation density was used as the integral intensity of (111) planes and the mean value of θ–fiber orientation density as the intensity of (001) planes. The trend line corresponding with the following logarithmic equation gives a correlation of 97 % as shown in Figure 11.

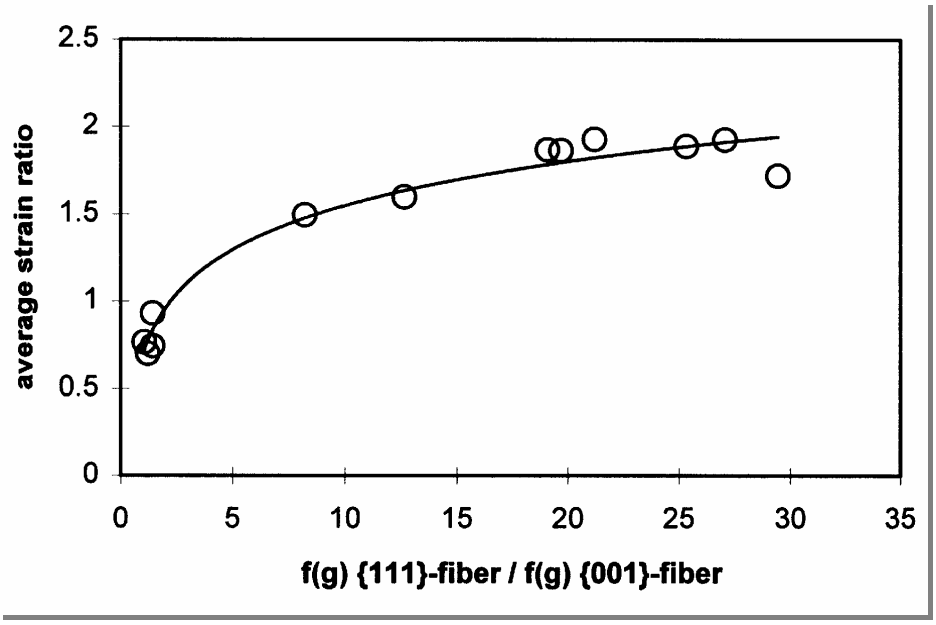

Figure 11. Empirical function relating the intensity ratio of (111) and (001) planes from texture measurement to the experimentally observed average strain ratio $\bar{r}$. The mean value of ?–fiber orientation density was here used as integral intensity of (111) planes and the mean value of ?–fiber orientation density as intensity of (001) planes. The trend line indicates the logarithmic equation $\bar{r}_{exper.} = 0.707 + 0.366 \times \ln\left(I_{(111)}/I_{(001)}\right)$.

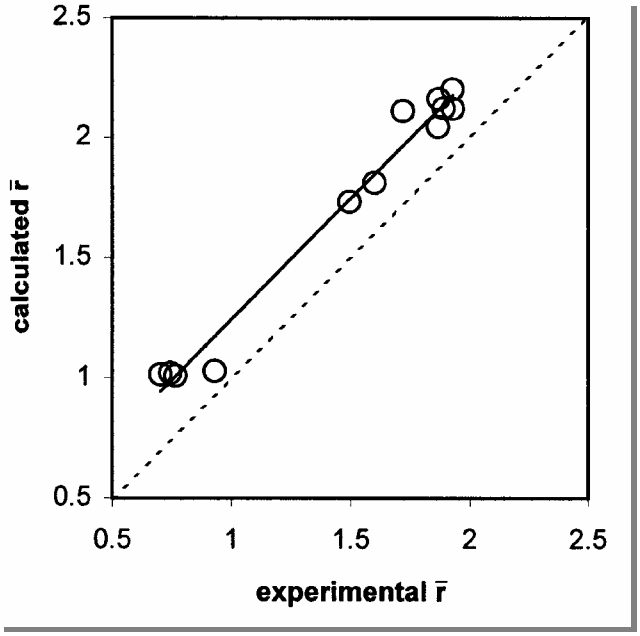

Figure 12. Empirical function relating experimental to theoretical anisotropy values. The calculations were made using a Taylor–Bishop–Hill type approach based on pencil glide. The linear empirical function matching this correlation is $\bar{r}_{calc.} = 1.006 \times \bar{r}_{exper.} + 0.238$.

$$\bar{r}_{exper.} = 0.707 + 0.366 \times \ln\left(I_{(111)} / I_{(001)}\right) \qquad (1)$$

Using the same experimental data, Figure 12 provides a direct linear correlation between the experimental and calculated average strain ratio $\bar{r}$. The calculations were done using a pencil glide Taylor–Bishop–Hill type model. The dotted trend line indicates a one–to–one correlation. A linear empirical function matching this correlation gives a correlation of even 98 %.

$$\bar{r}_{calc.} = 1.006 \times \bar{r}_{exper.} + 0.238 \qquad (2)$$

Equation 1 provides a decent correlation and shows that anisotropy of steel sheet can be roughly estimated by means of the intensities of (111) and (001) planes. However, equation 2 has the advantage of resembling a one–to–one ratio, and reveals an even higher correlation. This indicates that models of planar plastic anisotropy which account for the complete texture are superior for the evaluation of $\bar{r}$–values to models based on intensity ratios. Method 1 suffers particularly from the fact that large changes in the intensity ratio entail only small changes in the anisotropy prediction. This renders industrial–scale predictions which require accuracy at least within a 5 % window less reliable.

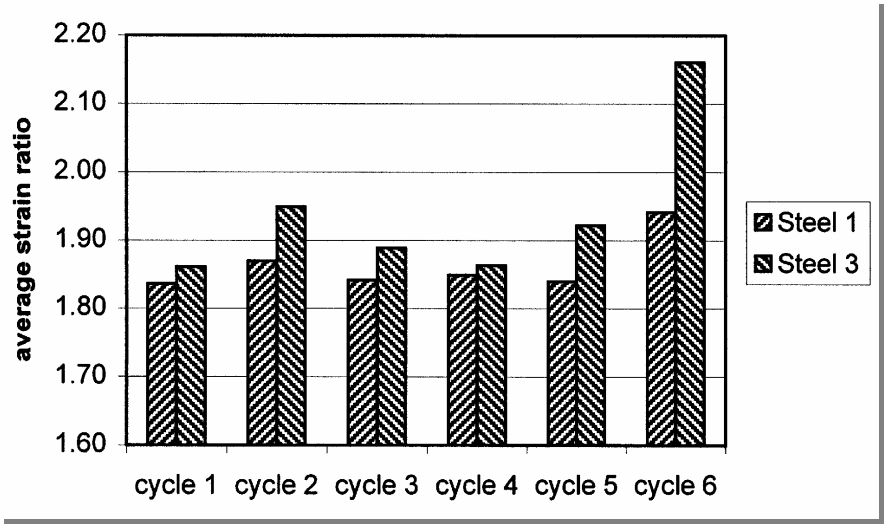

Figure 13. Calculated and corrected $\bar{r}$–values for all annealing cycles for steels 1 and 3. The first column represents the results of the theoretical calculation after correction by equation 2 for steel 1 and the second column for steel 3.

Using this result, $\bar{r}$–values of the recrystallized steels were calculated and corrected by equation 2 to match experimental results. Figure 13 summarizes the calculated and corrected $\bar{r}$–values for all annealing cycles for steels 1 and 3. The first column represents the results of the Taylor–Bishop–Hill calculation after correction by equation 2 for steel 1 and the second column for steel 3. It is shown that cycle 6 provides the best $\bar{r}$–value for steel 3, exceeding the $\bar{r}$–value of the other steel and the other cycles in average by about 13 %. The differences between various cycles were smaller for steel 1. However, cycle 6 also yielded the best results for steel 1 producing a slightly higher anisotropy ratio compared to the other annealing conditions.

V. Conclusions

The crystallographic texture and plastic anisotropy of five industrially produced IF steels was investigated. For optimization of texture, sheet isotropy, and homogeneity cold rolled specimens were additionally exposed to different annealing cycles resembling industry–scale continuous annealing conditions. Different methods were suggested for deriving anisotropy parameters both theoretically and experimentally. The main results are:

1. Hot band textures of IF steels hot rolled in the austenitic region were nearly random due to phase transformation and partial recrystallization. Slight differences between center and sub–surface textures can be explained by the through–thickness shear and temperature profile.

2. Cold rolling textures were typical plane-strain deformation textures. In the center layers, the α–fiber components were slightly enhanced compared to the sub–surface layer. The differences can be explained in terms of corresponding differences in the hot band.

3. Recrystallization textures were slightly sharper in sub–surface layers than in center layers. This was attributed to the deformation and orientation path history of cold rolling texture components and the texture inherited from the hot band.

4. Best agreement between experimental and theoretical anisotropy parameters was obtained by correcting theoretical anisotropy parameters derived by use of pencil glide based Taylor–Bishop–Hill theory with a linear fitted function derived using a compilation of experimental data.

5. Average strain ratio $\bar{r}$ could be increased by about 13 % simply by an adequate adjustment of annealing conditions in laboratory simulated continuous annealing. The annealing cycle with the highest maximum temperature produced the sharpest γ–fiber and therefore highest $\bar{r}$-values. The effect was stronger in a steel with higher carbon content and might result from partial transformation to austenite (intercritical annealing).

References

[1] G.I. Taylor: Journ. Inst. Met. 62 (1938) No. 1, p. 307/324.

[2] J.F. W. Bishop and R. Hill: Philos. Mag. 42 (1951) No. 327, p. 414/427.

[3] H.J. Bunge: Kristall u.Technik 5 (1970) p. 145/156.

[4] D. Raabe: Comput. Mater. Science 19 (2000) 13/26.

[5] W.B. Hutchinson: International Metals Reviews 29 (1984) No. 1, p. 25/42.

[6] H.J. Bunge: Theoretical Methods of Texture Analysis, DGM Informationsgesellschaft, Deutsche Gesellschaft für Metallkunde, 1987

[7] M. Hölscher, D. Raabe, and K. Lücke: Steel Research 62 (1991) No. 12, p. 567/575.

[8] U.F. Kocks, C.N. Tomé, H.-R. Wenk: Texture and Anisotropy, Cambridge University Press, 1998

[9] S. Mishra C., Därmann, K. Lücke: Acta Metall. 32 (1984) No. 12, p. 2185/2201.

[10] U. v. Schlippenbach, F. Emren and K. Lücke: Acta Metall. 34 (1986) No. 7, p. 1289/1301.

[11] M. Hölscher, D. Raabe and K. Lücke: Acta Metall. 42 (1994) No. 3, p. 879/886.

[12] H. Honneff and H. Mecking: Proc. ICOTOM 6, Tokyo, ISIJ (1981), p. 347/352.

[13] J.L. Raphanel and P. van Houtte: Acta Metall. 33 (1985) No. 8, p. 1481/1488.

[14] D. Raabe: Mater. Sc. and Technol. 11 (1995) No. 5, p. 455/460.

[15] D. Vanderschueren, L. Kestens, P. van Houtte, E. Aernoudt, J. Dilewijns and U. Meers: Mater. Sc. and Technol. 6 (1990) No. 12, p. 1247/1250.

[16] D. Raabe: Materials Science and Engineering A197 (1995) No. 1, p. 31/37.

[17] L. Tóth, A. Molinari and D. Raabe: Metallurgical Transactions A 28A (1997) No. 11, p. 2343/2351.

[18] W.B. Hutchinson, K. Ushioda: Scand. J. of Metallurgy 13 (1984) p. 269/284.

[19] W.B. Hutchinson: Acta Metall. 37 (1989) No. 4, p. 1047/1056.

[20] D. Raabe, K. Lücke: Scripta Metall. 26 (1992) No. 1, p. 19/24.

[21] D. Raabe, K. Lücke: Steel Research 63 (1992) No. 10, p. 457/464.

[22] Y.B. Park, D.N. Lee, G. Gottstein: Acta Materialia 44 (1996) No. 8, p. 3421/3427.

[23] U. Köhler, H.J. Bunge: Textures and Microstructures 23 (1995) p. 87/96.

[24] B. Samajdar, B. Verlinden, P. van Houtte: Acta Materialia 46 (1998) No. 8, p. 2751/2763.

[25] Y. Hayakawa, J.A. Szpunar: Acta Materialia 45 (1997) No. 9, p. 3721/3730.

[26] L. Kestens, J.J. Jonas: Metallurgical and Materials Transactions 27A (1996) No. 1, p. 155/164.

[27] D. Vanderschueren, N. Yoshinaga, K. Koyama: ISIJ International 36 (1996) No. 8, p. 1046/1054.

[28] C. Klinkenberg, D. Raabe and K. Lücke: Steel Research 63 (1992) No. 6, p. 263/269.

[29] C. Klinkenberg, D. Raabe and K. Lücke: Steel Research 64 (1993) No. 5, p. 262/266.

[30] L.G. Schulz: Journ. Appl. Phys. 20 (1949) No. 11, p. 1030/1036.
[31] H.J. Bunge: Z. Metallkunde. 56 (1965) No. 12, p. 872/874.
[32] D. Raabe; Lücke, K.: Materials Science Forum 157–162 (1994) p. 597/610.
[33] D. Raabe: Texturen kubisch–raumzentrierter Übergangsmetalle, RWTH Aachen, 1992, Dissertation.
[34] D. Raabe and K. Lücke: Scripta Metall. 26 (1992) No. 8, p. 1221/1226.
[35] D. Raabe and K. Lücke: Proceedings of International Conference on Strip Casting, Hot and Cold Working of Stainless Steels, Quebec, Canada, 1993, ed.N.D. Ryan, A.J. Brown, H.J. McQueen, The Metallurgical Society of the Candian Institute of Materials (CIM), p. 221/235.
[36] A. Fedosseev, D. Raabe, G. Gottstein: Materials Science Forum 157–162 (1994) p. 1771/1776.
[37] A. Fedosseev, D. Raabe: Scripta metall. 30 (1994) No. 1, p. 1/6.
[38] D. Raabe, K. Lücke: Proceedings of the 4th European Conference on Advanced Materials and Processes, Euromat 95, Padua/Venice, Italy, 25.-28. September 1995, Volume 3, Symposium F – Materials and Processing Control, Associatione Italiana di Metallurgia, Milano, Italy, p. 285/288.
[39] D. Raabe: Journal of Materials Science 30 (1995) No. 1, p. 47/52.
[40] D. Raabe: Metallurgical and Materials Transactions A 26A (1995) No. 4, p. 991/998.
[41] D. Raabe: Materials Science and Technology 11 (1995) No. 5, p. 461/468.
[42] D. Raabe: Physica Status Solidi (a) 149 (1995) p. 575/581.
[43] D. Raabe., F. Roters, V. Marx: Textures and Microstructures 26–27 (1996) p. 611/635.
[44] D. Raabe: Steel Research 66 (1995) No. 5, p. 222/229.
[45] N. Yurioka and T. Kasuya: Welding in the World 35 (1995) No. 5, p. 327/334.